Ablation of hematopoietic stem cell derived adipocytes reduces tumor burden in syngeneic mouse models of high-grade serous carcinoma

Elizabeth R Woodruff[1*], Courtney A Bailey[1,2*], Francis To[1], Vyshnavi Manda[3], Joanne K Maltzahn[4%], Timothy M Sullivan[4%], Meher P Boorgula[5,6], Maria Sol Recouvreux[7], Ruby Vianzon[8^], Bogi Conrad[8^], Kathleen M Gavin[8], Kimberly R Jordan[9], Dwight J Klemm[4,10], Sandra Orsulic[7], Benjamin G Bitler[1], Zachary L Watson[1#]

1 Division of Reproductive Sciences, Department of Obstetrics & Gynecology, University of Colorado School of Medicine, Aurora, CO 80045, USA

2 Biomedical Engineering Program, University of Colorado Boulder, Boulder, CO 80309, USA

3 Department of Medicine, University of Colorado School of Medicine, Aurora, CO 80045, USA

4 Department of Pulmonary Sciences and Critical Care, University of Colorado School of Medicine, Aurora, CO 80045, USA

5 University of Colorado Cancer Center, University of Colorado Anschutz Medical Campus, Aurora, CO 80045, USA

6 Department of Biomedical Informatics, University of Colorado Anschutz Medical Campus, Aurora, CO 80045, USA

7 Departments of Obstetrics & Gynecology and Pathology, and the Jonsson Comprehensive Cancer Center, David Geffen School of Medicine at UCLA, Los Angeles, CA 90095, USA

8 Division of Geriatric Medicine, Department of Medicine, University of Colorado School of Medicine, Aurora, CO 80045, USA

9 Department of Immunology and Microbiology, University of Colorado School of Medicine, Aurora, CO 80045, USA

10 Geriatric Research, Education and Clinical Center, Rocky Mountain Regional Veterans Administration (VA) Medical Center, Aurora, CO 80045, USA

* **Co-First Authors: ERW and CAB contributed equally**

% JKM and TMS contributed equally

^ RV and BC contributed equally

Corresponding Author

Zachary L. Watson

Division of Reproductive Sciences

Department of Obstetrics & Gynecology

12700 E. 19th Ave., MS8613

Aurora, CO 80045

Phone: (303) 724-8682

Fax: (303) 724-3512

zachary.watson@cuanschutz.edu

Word count: 6900 (excluding abstract and references)

Figure count: 5

Table count: 2

Supplemental figure count: 6

Supplemental table count: 6

ABSTRACT

In this study we examined the influence of hematopoietic stem cell-derived adipocytes (HSCDAs) on the proliferation and metastasis of high-grade serous carcinoma (HGSC) – the most common type of ovarian cancer. HSCDAs are a subtype of adipocytes that differentiate from myeloid precursors that traffic from bone marrow to adipose tissue and accumulate therein. These are distinct from conventional mesenchymal adipocytes (CMAs), which are derived from mesenchymal precursors. We hypothesized that HSCDAs promote HGSC progression and establish a pro-tumoral niche within peritoneal adipose tissues such as the omentum.

Primary human white adipose tissue samples were obtained via biopsy and then sorted into myeloid and mesenchymal populations through flow cytometry. These adipose precursors were then differentiated *in vitro* into mature HSCDAs and CMAs, respectively. Transcriptomic analysis showed that HSCDAs have a distinct transcriptional profile from CMAs, including downregulation of cell cycle and upregulation of multiple metabolic and adipogenic pathways. Using ELISA, we found that HSCDAs secreted greater amounts of inflammatory cytokines IL-6 and IL-8 than CMAs. Next, we incubated HGSC cells in conditioned media from HSCDAs and CMAs and performed proliferation and protein expression profiling. HGSC cells in HSCDA media, compared to those in CMA media, had elevated expression of protein markers related to epithelial to mesenchymal plasticity, including fibronectin, as well as increased serine phosphorylation of pro-survival AKT1/2. Conversely, HGSC cells in HSCDA media exhibited comparably downregulated expression of tumor suppressors including the Wnt regulator GSK3β. Depending on the cell line and adipose donor, HGSC cells also showed altered growth rates in conditioned media.

We next investigated the role of HSCDAs in HGSC progression and metastasis *in vivo*. We generated immunocompetent mice that were either HSCDA Proficient (can make both adipocyte subtypes) or Deficient (can only make CMAs). Using these models, we conducted two independent tumor studies using the ID8 (*Tp53-/-*, *Brca2-/-*) and SO (*Tp53-/-*, *Brca1/2* wild-type, *Hras* and *Myc* amplified) syngeneic models. Overall tumor burden was lower in HSCDA Deficient mice in both models. In the ID8 model, omental tumors from HSCDA Deficient mice showed reduced proliferation (Ki67) and apoptosis (cleaved caspase 3) relative to those from Proficient mice.

Transcriptionally, omental ID8 tumors from HSCDA Deficient downregulated oxidative phosphorylation, adipogenesis, and fatty acid metabolism relative to tumors from HSCDA Proficient mice. These pathways were

enriched in HSCDA cells *in vitro*, suggesting that ablation of HSCDAs had a significant influence on the tumor metabolic environment. Reduced inflammatory pathways in ID8 tumors from HSCDA Deficient mice were also observed leading us to interrogate immune cell infiltration into omental tumors. Compared to HSCDA Proficient mice, tumors from HSCDA Deficient mice showed reduced densities of dendritic cells (DC) and natural killer (NK) cells, as well as fewer DCs, NKs, and B-cells in proximity to tumor cells, as determined by spatial analysis. Overall, our data suggest that HSCDAs promote HGSC survival and plasticity while downregulating expression of tumor suppressors and altering the peritoneal immune and metabolic environment to promote HGSC progression.

BACKGROUND

Most ovarian cancer cases are of the high-grade serous subtype (high grade serous carcinoma; HGSC) [1]. HGSC preferentially invades visceral adipose tissues (VAT) such as the omentum [2-5], a complex apron-like fold of the visceral peritoneum that lies across the anterior aspect of the intestines. It is primarily composed of adipocytes surrounded by a mesothelial layer but also contains vasculature and “milky spots,” small tertiary lymphoid aggregates that may be innervated sympathetic nervous system fibers [6, 7]. Omental tumors are often the largest abdominal tumors in women with ovarian cancer, suggesting that the microenvironment of the omentum is highly conducive to HGSC cell invasion and proliferation. Adipocytes actively enhance HGSC metastasis through several mechanisms, including but not limited to: (a) secretion of inflammatory cytokines, such as IL-8, promoting HGSC migration and invasion, (b) providing energy to HGSC cells through direct lipid transfer, and (c) stimulating upregulation of fatty acid binding protein 4 (FABP4), fatty acid translocase (CD36), and other regulatory proteins of fatty acid transport and lipid metabolism [8-10].

Peritoneal adipose tissue (AT) remodeling during menopause may result in chronic inflammation and a pro-tumoral niche. Relative to premenopausal women, postmenopausal women have an increased risk of developing HGSC and a two-fold increase in peritoneal metastases at diagnosis [11], but many mechanisms driving these phenomena remain poorly understood. During aging, visceral adiposity may increase through the enlargement of existing adipocytes (hypertrophy) and/or *de novo* production of new adipocytes (hyperplasia). Adipocytes were previously thought to be entirely of mesenchymal origin, but a 2006 mouse bone marrow transplant study showed that some myeloid cells traffic through the circulation, become resident in adipose tissue, and terminally differentiate into adipocytes [12]. A recent publication termed these cells hematopoietic stem cell-derived adipocytes (HSCDAs) [13] to distinguish them from conventional mesenchymal-derived adipocytes (CMAs). In 2015 and 2016, HSCDAs were identified in humans [14, 15]. Ryden et al. isolated mature white adipocytes from recipients of bone marrow transplants (BMT) and evaluated them for donor and recipient DNA. Up to 27% of purified adipocytes were derived from donor cells. The fraction of donor-derived adipocytes was positively correlated with time since transplant, and the percentage of donor cells in obese subjects was significantly higher than in non-obese individuals [14]. Gavin et al. performed a similar study and found that up to 35% of mature adipocytes were generated from donor cells in BMT recipients, and the proportion of donor DNA was positively correlated with elapsed time post-transplant [15]. These two independent studies confirmed

the existence of human HSCDAs and demonstrated that their proportion of total adipose cells increases with age.

Subsequent studies developed methods to isolate and differentiate human primary adipocyte precursors into HSCDA and CMA populations, as well as an innovative mouse HSCDA ablation model [13, 16-18]. These studies demonstrated that mouse HSCDAs accumulated with age and occurred in significantly higher numbers in female versus male mice. Transcription analysis showed that HSCDAs differ from CMAs by upregulation of inflammatory gene expression and decreased expression of leptin and lipid oxidation pathways [19]. Of key relevance to menopause and HGSC, mouse HSCDA production was found to be enhanced by models of "pseudomenopause" such as ovariectomy and estrogen receptor alpha knockout. HSCDA production in ovariectomized mice was attenuated by estradiol replacement, demonstrating that the ovarian hormone is necessary and sufficient for the constraint of HSCDA production. In agreement with prior anatomical studies, HSCDA accumulation in these mice was higher in visceral adipose tissue (VAT) and gonadal adipose tissue (GAT) compared to subcutaneous adipose tissue (SAT) depots [17]. Finally, depletion of HSCDAs in mice did not alter the quantities of tissue-resident immune cells in GAT or SAT depots; however, HSCDA depleted mice were found to have increased circulating leptin levels, indicating that the presence or absence of HSCDAs may alter lipid homeostasis [13].

Numerous studies have surveyed the effects of adipocytes on ovarian cancer progression, metastasis, and metabolism, but to date, none have compared the distinct influences of HSCDAs and CMAs. Given their presence in humans and their characteristics in mouse models, we predicted that HGSC cells would exhibit differential phenotypes in HSCDA and CMA cultures and media, and that HGSC tumors would show differential growth and spread in HSCDA deficient mice. In this study, we report that HGSC cells *in vitro* exhibit altered proliferation and protein expression in response to conditioned media from HSCDAs. We also report that ablation of HSCDA production in mice results in reduced HGSC tumor burden and multiple changes in tumor transcription and immune microenvironment.

RESULTS

Compared to CMAs, cultured human HSCDAs exhibit differential transcription and cytokine secretion

Prior transcriptomic data from mouse HSCDAs and CMAs showed that the former exhibit a highly inflammatory transcriptional profile compared to the latter, including increased mRNA expression of *Cxcl10*, *Mcp1*, *Il6*, and *Cxcl1* [19]. We hypothesized that *in vitro* cultured human HSCDAs would also exhibit unique transcription profiles. We collected adipose biopsies from human female donors (menopause status is shown in **Supplementary Table ST1**) and flow sorted cells into myeloid and mesenchymal populations [18] and then differentiated these adipose precursors into HSCDAs and CMAs, respectively. **(Fig. 1A)** We then performed RNA-Seq on matched HSCDA/CMA pairs from three independent donors (Donors 1-3). Principal component analysis (PCA) showed that cells from Donor 1 and Donor 3 clustered together, while HSCDAs and CMAs did not cluster for Donor 2 **(Fig. 1B** and **Supplementary Fig. S1)**. Next, we examined differential gene expression (DGE, **Fig. 1C**) and performed over-representation analysis (ORA) for Hallmark pathways. Multiple cell cycle pathways, including E2F Targets, Mitotic Spindle, and G2M Checkpoint, were decreased in human HSCDA cells **(Fig. 1D-E)**. Gene set enrichment analysis (GSEA) recapitulated downregulation of these three pathways **(Supplementary Fig. S2A-B)**. Highlighted genes in these pathways include LMNB1 and CDK1 **(Fig. 1C)**. GSEA also revealed enrichment in HSCDAs for multiple Hallmark metabolic pathways, including Oxidative Phosphorylation, Adipogenesis, and Fatty Acid Metabolism **(Supplementary Fig. 2C-E)**.

While we did not observe transcriptional differences in inflammatory cytokines, we hypothesized that secretion may differ between human HSCDAs and CMAs. We analyzed conditioned media from paired HSCDAs and CMAs from six independent human female donors (Donors 4-9) using a multiplex ELISA for 10 cytokines (IFN-γ, IL-1β, IL-2, IL-4, IL-6, IL-8, IL-10, IL-12p70, IL-13, and TNF-α). HSCDAs from four donors secreted higher concentrations of IL-6, while five secreted higher concentrations of IL-8 **(Fig. 1F-K)**. Averaged across all six donors, HSCDA media contained 5.7-times the concentration of IL-6, and 6.7-times the concentration of IL-8, compared to paired CMA media. The remaining cytokines were not detected within the range of the assay. Overall, these experiments demonstrate that compared to human CMAs, human HSCDAs exhibit a different transcriptional profile and secrete greater amounts of inflammatory cytokines.

Conditioned media from HSCDAs alters protein expression and phosphorylation in HGSC cells

We hypothesized that HGSC cells may exhibit differential protein expression and/or phosphorylation in response to paracrine cytokine signaling from HSCDAs or CMAs. We took conditioned media from paired

HSCDA and CMA cells from four independent human female donors (Donors 6-9) and incubated them on PEO1 cells (a HGSC cell line, *TP53* mutant, *BRCA2* mutant) for 24 h. Protein expression and phosphorylation in the PEO1 cells was analyzed by reverse phase protein array (RPPA) **(Fig. 2A)**. Relative to cells in CMA media, PEO1 incubated in HSCDA media showed upregulated fibronectin **(Fig. 2B)**, glyceraldehyde 3-phosphate dehydrogenase (GAPDH), and tissue transglutaminase 2 (TG2) **(Fig. 2A)** across all four donors. Additionally, we observed increased serine phosphorylation of multiple kinases, including AKT1-pS473 **(Fig. 2A)**, AKT2-pS474 **(Fig. 2A, F)**, and p21-activating kinase 4 (PAK4-pS474, **Fig. 2A,D**,). PEO1 cells in HSCDA media, relative to cells in CMA media, also showed consistent downregulation of multiple tumor suppressors, including the regulatory p85 subunit of PI3K (PI3K-p85), protein tyrosine phosphatase non-receptor type 12 (PTPN12), programmed cell death protein 4 (PDCD4) **(Fig. 2A)**, and glycogen synthase kinase 3 beta (GSK3β) **(Fig. 2C).** Notably, while phosphorylated forms of PAK4 **(Fig. 2D)** and AKT2 **(Fig. 2F)** were found at higher levels, the total forms of these proteins **(Fig. 2E,G)** were not differentially expressed between treatment groups, highlighting specific differences in serine phosphorylation in the absence of overall protein changes.

Because HSCDAs secreted more IL-6 and IL-8, we next explored whether PEO1 cells directly respond to IL-6 and/or IL-8 exposure. Using RT-qPCR to assay mRNA expression of IL-6 receptors (*IL6R* and *IL6ST*) and IL-8 receptors (*CXCR1* and *CXCR2*) in PEO1 cells, we observed robust expression of *IL6ST*, but low or no expression of the other receptors **(Fig. 2H)**. We then used flow cytometry to examine surface protein expression. In concordance with RT-qPCR, we found that over 80% of PEO1 cells expressed IL6ST, but very few cells expressed IL6R, CXCR1, or CXCR2 **(Fig. 2I)**. Finally, we incubated PEO1 cells directly in recombinant IL-6, IL-8, or both for one hour and performed immunoblot for resultant intracellular signaling (phosphorylated STAT3 for IL-6; phosphorylated ERK1/2 for IL-8). There were no differences in either p-STAT3 or p-ERK1/2 **(Fig. 2J)**. We observed similar results for RT-qPCR, flow cytometry, and immunoblot in two other HGSC cell lines, OVCAR4 (*TP53-/-*, *BRCA1/2* wild-type) and OVCAR8 (*TP53-/-*, *BRCA1/2* wild-type*, ERBB2* mutant, *KRAS* mutant, *CTNNB1* mutant) **(Supplementary Fig. S3)**. Overall, these data show that HGSC cells exhibit differential protein expression and phosphorylation in response to paracrine signaling from HSCDA and CMA adipocyte subtypes and that this differential response is not likely to be driven by IL-6 or IL-8 directly.

Conditioned media from HSCDAs alters the growth kinetics of HGSC cells

We next hypothesized that HGSC cells would exhibit differential proliferation rates when cultured in HSCDA or CMA conditioned media. We incubated PEO1, OVCAR4, and OVCAR8 cells in HSCDA or CMA conditioned media, each sourced from one of five independent human female donors (Donors 5-9). The media were paired such that HSCDA and CMA conditioned media from each donor were matched for direct comparison. Proliferation was monitored using IncuCyte live imaging **(Fig. 3)**. PEO1 cells showed increased proliferation in HSCDA media compared to CMA media from 2 of 5 donors (Donors 5 and 9), with no significant changes in the remaining 3 donors (Donors 6-8). OVCAR4 cells showed relatively decreased proliferation in HSCDA media from Donor 6 and increased proliferation in HSCDA media from Donor 9, while the other media pairs showed no significant differences. OVCAR8 cells exhibited increased proliferation in HSCDA media from Donor 5 and unchanged proliferation in the other media pairs. These results indicate that HGSC cells can exhibit differential growth in response to paracrine signaling from HSCDA or CMA adipocyte subtypes in a cell line- and donor-dependent manner.

Ablation of HSCDAs attenuates tumor burden in two independent syngeneic murine models of HGSC

We have demonstrated that incubation in HSCDA conditioned media, relative to CMA conditioned media, alters protein expression and proliferation rates of HGSC cells **(Fig. 2-3)**. Additionally, we showed that HSCDAs secrete greater amounts of inflammatory cytokines IL-6 and IL-8 than CMAs **(Fig. 1F-K)**. Both IL-6 and IL-8 have been shown to increase the metastatic and invasive capabilities of HGSC cells [9, 20, 21]. Adipocytes also alter the tumor metabolic environment and enhance tumor cell proliferation by providing energy through lipid transfer and stimulating HGSC cell fatty acid metabolism [8-10]. We therefore hypothesized that ablation of HSCDAs in mice may reduce tumor progression in syngeneic models of HGSC. To specifically ablate HSCDAs, irradiated C57BL/6J recipient mice were transplanted with hematopoietic stem cells (HSC) from donor mice in which a mature adipocyte-specific adiponectin gene promoter controls expression of an attenuated diphtheria toxin (DTA) gene. This approach ablates any HSC that differentiates into an adipocyte by endogenous DTA expression, thereby abrogating HSCDA production in the recipient mice. Importantly, CMAs are unaffected by myeloablation and transplant, as they are derived from host mesenchymal precursors that do not express the DTA construct. We refer to this mouse cohort as “HSCDA Deficient.” Control mice were generated by transplanting HSCs from

donor mice encoding a reporter gene but lacking DTA allowing the production of both HSCDAs and CMAs from hematopoietic and mesenchymal precursors, respectively. We refer to this mouse cohort as “HSCDA Proficient”.

Following a six-week recovery from HSC transplantation, HSCDA Deficient and Proficient mice were engrafted with ID8 (*Tp53-/-*, *Brca2-/-*, GFP-Luc+) cells by intraperitoneal (IP) injection **(Fig. 4A)**. At 39 days post-implantation, tumor-bearing mice were euthanized, and necropsy was performed to assess tumor burden and collect specimens for downstream analyses of the tumor and peritoneal environment. Total omentum weight was lower in HSCDA Deficient mice compared to HSCDA Proficient mice **(Fig. 4B)**. The number of disseminated tumor nodules within the mesentery and other peritoneal locations **(Fig. 4C)** and the total mass per mouse of these tumor nodules **(Fig. 4D)**, were also lower in HSCDA Deficient mice. Representative images of the peritoneal space, including GFP+ tumors, are shown for HSCDA Proficient **(Fig. 4E)** and Deficient **(Fig. 4F)** mice. Consistent with previous studies performed by our group [22], the largest tumors were found on the omenta **(Fig. 4E-F)**.

Given the reduced overall tumor burden in HSCDA Deficient mice, we performed immunohistochemistry (IHC) on omental tumor sections to determine if tumor cell proliferation and apoptosis were affected by HSCDA status. Representative images of Ki67 (proliferation) and cleaved caspase 3 (apoptosis) are shown in **Fig. 4G** and **Fig. 4H**, respectively. Consistent with reduced tumor burden, the percentage of Ki67 positive tumor cells was lower in HSCDA Deficient mice (average = 8.4%) than in HSCDA Proficient mice (average = 11.1%) **(Fig. 4I)**, demonstrating slowed tumor proliferation and suggesting that the peritoneal adipose environment may be less conducive to tumor growth. The percentage of cleaved caspase 3 positive tumor cells was also lower in HSCDA Deficient mice (average = 1.2%) than in HSCDA Proficient mice (average = 2.2%) **(Fig. 4J)**.

To examine the peritoneal adipokine milieu of tumor-bearing mice, we collected a portion of ascites fluid during necropsy. Cells were removed by centrifugation, and adipokine concentrations in the supernatant were analyzed using a multiplex ELISA for mouse BDNF, IL-1β, IL-6, IL-10, Insulin, Leptin, MCP-1, and TNF-α. All adipokines were detected within the assay range. No HSCDA-dependent effects on measured adipokine concentrations reached statistical significance **(Supplementary Fig. S4A-H)**.

As further confirmation of the effects of HSCDA ablation, we performed a second tumor study in HSCDA Proficient and Deficient mice using the “SO” model [a kind gift from the Sandra Orsulic laboratory, UCLA]. SO cells are *Tp53-/-*, Brca1/2 wild-type, $Hras^{V12}$ and *Myc* amplified. After an 8-week recovery of mice from

myeloablation and bone marrow transplant, SO cells were implanted by IP injection. The SO model formed large solid omental and peritoneal tumors very rapidly, leading to the euthanization of the mice after 20 days. Consistent with the ID8 model, we observed reductions in omental tumor weight and the number and mass of non-omental peritoneal tumors **(Supplementary Fig. S5)**. Collectively, the ID8 and SO studies demonstrate that ablation of HSCDAs reduces intraperitoneal tumor burden in two independent syngeneic HGSC models, both in terms of omental and non-omental tumor mass as well as the number of additional metastatic sites.

HSCDA ablation alters transcription and the immune microenvironment in ID8 tumor-bearing mice

The ablation of HSCDAs in two immune intact HGSC models led to reduced tumor burden **(Fig. 4)**, thus we next assessed the HSCDA-dependent transcriptome and tissue architecture. We conducted transcriptomic analysis of omental tumors from HSCDA Proficient (n=4) and HSCDA Deficient (n=4) mice to characterize the transcriptional profiles of the tumor microenvironment. PCA showed broad clustering of HSCDA Proficient (blue) and Deficient (red) groups **(Fig. 5A)**. DGE analysis revealed a trend toward upregulation of gene expression in HSCDA Deficient mice relative to HSCDA Proficient controls **(Fig. 5B)**. GSEA analysis identified multiple differentially regulated Hallmark pathways **(Fig. 5C)**. Notably, three pathways enriched in human HSCDA cultures – Oxidative Phosphorylation, Adipogenesis, and Fatty Acid Metabolism – were depleted in HSCDA Deficient mice **(Fig. 5C** and **Supplementary Fig. S6)**, suggesting that HSCDA depletion had altered the metabolic environment of the omentum.

GSEA analysis also revealed the depletion of multiple immune-related Hallmark pathways, including Allograft Rejection, Inflammatory Response, and IL-2 STAT5 Signaling **(Fig. 5D-F)**. We then performed multiplex IHC (mIHC) on omental tumors to assess whether HSCDA status affected the tumor immune microenvironment. Tissue sections were stained using two separate panels of antibodies, both of which included staining for nuclei (DAPI) and tumor cells (transcription factor WT1). The “innate” panel **(Table 1)** detected myeloid cells including dendritic cells (DC), natural killer cells (NK), macrophages, and subpopulations of myeloid derived suppressor cells (MDSCs). The “adaptive” panel **(Table 2)** detected lymphoid cells including B-cells and several subtypes of T-cells. **Fig. 5G** shows a representative multicolor image of an omentum tumor stained with the “innate” panel. After tissue and cell segmentation, cell densities were quantified in regions of interest. We found that the densities of DCs (CD11c+) and NKs (CD49b+/CD31-) were significantly lower in omental tumors from HSCDA

Deficient mice compared to HSCDA Proficient mice **(Fig. 5H)**. Following the cell density analysis, we performed spatial analysis to calculate the number of each immune cell type within 50 microns of WT1+ tumor cells. Within this radius, the numbers of B-cells (B220+), DCs (CD11c+), and NKs (CD49b+/CD31-) were reduced in the omental tumors of HSCDA Deficient mice **(Fig. 5I)**. These analyses show that HSCDA ablation affected not only tumor burden and bulk transcription but also the tumor immune microenvironment.

DISCUSSION

Human data suggest that the proportion of HSCDAs increases over time. [15]. In mouse models, HSCDAs preferentially accumulate in VAT and GAT depots, and their production is inversely correlated with estrogen signaling [17]. Crucially, most ovarian cancer diagnoses occur post-menopause [23], and the aged peritoneal microenvironment can be highly conducive to ovarian cancer progression [24]. We broadly hypothesized that HSCDAs may promote HGSC progression by establishing a pro-tumor niche within VAT, such as the omentum, a site of particularly high HGSC dissemination in human cases.

HSCDAs have a distinct transcriptional profile compared to CMAs, including the downregulation of Hallmark cell cycle pathways **(Fig. 1B-E)** and upregulation of multiple metabolic pathways, including Oxidative Phosphorylation, Adipogenesis, and Fatty Acid Oxidation **(Supplementary Fig. S2)**. ELISA of adipocyte conditioned media showed that human HSCDAs secrete higher amounts of IL-6 and IL-8 than CMAs **(Fig. 1F-K)**. Our RPPA data **(Fig. 2A-G)** indicated that HGSC cells in HSCDA media, relative to CMA media, exhibit upregulated tissue transglutaminase 2, which has been associated with epithelial-to-mesenchymal plasticity (EMP) in ovarian cancer [25, 26], as well as fibronectin, which is broadly associated with EMP in multiple cancer types [27]. Serine phosphorylation was also elevated in these cells, including pro-survival AKT1, AKT2, and PAK4, a group II serine/threonine protein kinase that can regulate cytoskeletal remodeling [28, 29] and Wnt/β-catenin signaling [30]. Interestingly, we observed that PEO1 cells cultured in HSCDA conditioned media exhibited downregulated GSK3β, a tumor suppressor and negative regulator of Wnt/β-catenin signaling. Other downregulated tumor suppressors included PTPN12, a tyrosine phosphatase that regulates PTEN and AKT signaling and suppresses the migration of ovarian cancer cells [31, 32], and PDCD4, a pro-apoptotic tumor suppressor with clinical significance in gliomas and colorectal cancers [33, 34].

While adipocyte-derived IL-6 and IL-8 have been shown to promote ovarian cancer survival, metastasis, and chemoresistance [9, 35], our data show that PEO1, OVCAR4, and OVCAR8 cells in culture express low levels of IL-6 receptor (IL6R) and IL-8 receptors (CXCR1 and CXCR2) **(Fig. 2H-J** and **Supplementary Fig. S3)**. It is therefore likely that additional signaling mechanisms regulate the observed differences in HGSC cell proliferation and protein expression in HSCDA media. Prior studies have shown that exosomes from human omentum conditioned media can increase the proliferative and invasive capacity of ovarian cancer cells [36], and microRNAs from adipose tissue-derived exosomes can regulate gene expression in non-adipose tissues [37, 38]. Both PTPN12 and PDCD4, tumor suppressors that were downregulated in PEO1 cells in HSCDA media **(Fig. 2A)**, are regulated by microRNA miR-503 [39, 40]. Future work examining the contribution of exosome-derived factors, including microRNAs, may reveal a mechanism for our observations.

Results from our *in vivo* studies in two independent syngeneic HGSC models showed that ablation of HSCDAs reduced overall tumor burden **(Fig. 4B-F, Supplementary Fig. S5)**. Reduced Ki67 positivity in tumor cells from HSCDA Deficient mice suggests that lower tumor burden may be due to slowed proliferation **(Fig. 4G,I)**. Bulk RNA-Seq of ID8 omentum tumors revealed that HSCDA ablation caused a reduction in Hallmark pathways Oxidative Phosphorylation, Adipogenesis, and Fatty Acid Oxidation **(Supplementary Fig. S6)**, all of which were upregulated in human HSCDA cultures **(Supplementary Fig. S2)**. Combined with the observed reduction in tumor burden and reduced Ki67, these data strongly suggest that the peritoneal metabolic environment of HSCDA Deficient mice was less supportive of tumor cell metastasis and growth. The proportion of cleaved caspase 3-positive tumor cells was also reduced in HSCDA Deficient mice, suggesting lower levels of ongoing apoptosis **(Fig. 4J)**. Whether this reduction is due to decreased tumor killing by immune cells or other causes remains to be determined.

RNA-Seq of omentum ID8 tumors also revealed downregulation of multiple immune-related pathways **(Fig. 5C-F)**. Omental tumors in HSCDA Deficient mice showed reduced density of dendritic cells and natural killer cells, as well as fewer DCs, NKs, and B-cells within a 50 μm radius of tumor cells **(Fig. 5G-I)**. Innate immune cells such as NKs and DCs can directly target malignant cells and broadly promote the recruitment of adaptive immune cells, and it has been proposed that B-cells also promote the HGSC anti-tumor response [41]. However, tumor-promoting roles have also been described for each of these cells. For example, tumor microenvironment components can suppress NK cell cytotoxicity and induce angiogenesis [42]. In a study of murine

adenocarcinoma and melanoma, NK cells rapidly lost effector functions after entering the tumor environment [43]. Additionally, regulatory B-cells can suppress immune response through the production of anti-inflammatory cytokines [44, 45]. Further exploration is needed to characterize the populations of tumor infiltrating DCs, NKs, and B-cells, and whether the balance of pro- or anti-tumor cells can be shifted by the presence of HSCDAs.

In conclusion, ovarian cancer aggressively invades adipose tissues, including the omentum, and numerous studies have highlighted the role of adipocytes in promoting tumor progression. Here we present the first study interrogating interactions between HSCDAs and ovarian cancer cells, as well as two independent *in vivo* tumor studies comparing HSCDA Deficient and Proficient mice. Overall, our results suggest HSCDAs are important contributors to ovarian cancer progression. HSCDAs may downregulate tumor suppressors and enhance pro-survival and pro-EMP signaling pathways in HGSC cells. They may also alter the peritoneal immune and metabolic environment to establish a metastatic niche and promote disease progression.

MATERIALS AND METHODS

HGSC cell culture

PEO1 (RRID:CVCL_2686), OVCAR4 (RRID:CVCL_1627), and OVCAR8 (RRID:CVCL_1629) were obtained from the Gynecologic Tissue and Fluid Bank (GTFB) at the University of Colorado and were authenticated at the University of Arizona Genomics Core using short tandem repeat DNA profiling. Cells were confirmed free of mycoplasma using MycoLookOut PCR (Sigma) last evaluated on July 12, 2024. Standard culture conditions for these lines is 37 °C in 5% CO_2 in RPMI 1640 supplemented with 10% fetal bovine serum (FBS) and 1% penicillin/streptomycin.

Primary preadipocyte culture, adipogenic differentiation, and conditioned media collection

Primary mesenchymal and myeloid-derived adipocyte precursors were grown in 15 cm tissue culture plates in Growth Media (GM): Alpha-MEM (Corning #10-022-CV) supplemented with 10% FBS (Gemini #100-106) and 0.1% penicillin/streptomycin (Sigma #P4333). Upon confluence, cells were differentiated for seven days in Complete Differentiation Media (CDM): DMEM/F12 (Corning #10-092-CV) supplemented with 33 μM D-biotin (Sigma #B4639), 17 μM pantothenate (Sigma #P5155), 1 μM rosiglitazone (Fisher #NC9331406), 0.5 mM 3-isobutyl-1-methylxanthine (IBMX; Sigma #I5879), 2 nM 3,3',5-triiodo-L-thyronine (T3; Sigma #T6397), 10 μg/mL transferrin (Sigma #T8158), and 100 nM insulin (Sigma #I9278). Cultures were then maintained for seven days in adipocyte maintenance media (AMM): DMEM/F12 supplemented with 33 μM D-biotin, 17 μM pantothenate, and 10 nM insulin (same suppliers as CDM). At the end of the seven-day AMM period, media was removed from adipocyte cultures. Cells were gently washed with PBS, and then media was replaced with fresh AMM. After a 24-hour incubation, conditioned media was collected for use with HGSC cells or ELISA analysis.

Bulk RNA-Seq of human primary HSCDAs and CMAs

Total RNA was isolated from human primary HSCDA and CMA cultures using the RNeasy Plus kit (Qiagen). Library preparation and sequencing were performed by the University of Colorado Cancer Center Genomics Shared Resource (RRID: RRID:SCR_021984). Reads were analyzed by the University of Colorado Cancer Center Bioinformatics Core Facility (RRID:SCR_021983). RNA-Seq data were processed using the nf-core

RNAseq pipeline (version 3.12.0; [46]). Briefly, Illumina adapters were removed using Cutadapt (version 3.4; [47]) as part of the trimgalore (0.6.7) package [48]. Reads were aligned using STAR (version 2.7.9a; [49]) to the human transcriptome (GRCh38, gene annotation from Ensembl release 104) and quantified using Salmon (version 1.10.1; [50]). Raw data with counts by gene was generated using tximport ([51]) on salmon quantified data. Normalized data was generated to counts per million [52]. Differential expression was calculated between sample groups using the limma R package [53]. Gene set enrichment analysis (GSEA) was performed using fold-change and the fgsea R package [54] with Hallmark gene sets from the Molecular Signatures Database [55], which were downloaded using the msigdbr R package. Raw and processed RNA-Seq data was deposited in the Gene Expression Omnibus (GSE277309).

Multiplex ELISA

For human cytokines in conditioned media, AMM was incubated on HSCDA or CMA cells for 24 h, then collected. The concentration of 10 cytokines (IFN-γ, IL-1β, IL-2, IL-4, IL-6, IL-8, IL-10, IL-12p70, IL-13, and TNF-α) in conditioned media was measured using the V-PLEX Proinflammatory Panel 1 Human Kit (Meso Scale Diagnostics #K15049D).

For mouse adipokines, ascites fluid was collected from the peritoneal space of tumor-bearing HSCDA Proficient and Deficient mice using a needle and syringe. The supernatant was cleared of cells by centrifugation, and the concentrations of 8 adipokines (BDNF, IL-1β, IL-6, IL-10, Insulin, Leptin, MCP-1, and TNF-α) were measured in the supernatant using the U-PLEX Adipokine Combo 1 mouse kit (Meso Scale Diagnostics #K15299K).

Reverse Phase Protein Array (RPPA)

PEO1 cells were incubated for 24 h in conditioned media from four independent HSCDA or CMA cultures (see above for generation and collection of conditioned media). PEO1 cells were then washed briefly with PBS, collected, and snap frozen. Cell pellets were shipped to the MD Anderson Reverse Phase Protein Array Core (RRID:SCR_016649), which performed the assay.

Reverse-transcriptase quantitative PCR (RT-qPCR)

RNA was isolated from cells using the RNeasy Plus kit (Qiagen). mRNA expression was determined using SYBR green Luna One Step RT-qPCR Kit (New England BioLabs) on a Bio-Rad C1000 Touch thermocycler. Expression was quantified by the ΔCt method using target-specific primers and glyceraldehyde 3-phosphate dehydrogenase (*GAPDH*) control primers. mRNA-specific primers were designed to span exon-exon junctions to avoid the detection of genomic DNA. Primer sequences are shown in **Supplementary Table ST2**.

Flow cytometry

1 million HGSC cells grown in standard conditions (see above) were collected and resuspended in 100 µL of flow assisted cell sorting buffer (FACS buffer: Hank's Balanced Salt Solution [Corning #21-022-CV] with 2% FBS) and incubated in a 1:100 dilution of primary antibody for 20 minutes at 4 °C. Cells were then washed in 300 µL FACS buffer and centrifuged at 300 x *g* for 5 minutes. Cells were resuspended 300 µL FACS buffer and transferred to 5 mL tubes through 35 µm strainer caps (Falcon #352235). Full details of antibodies and isotype controls are given in **Supplementary Table ST3**. An Agilent Novocyte Penteon was used for detection and data were analyzed using FlowJo 10.8.1.

Immunoblotting

HGSC cells were seeded to sub-confluence in 10 cm dishes in standard media and allowed to settle overnight. Media was aspirated and cells were washed with PBS. Media was then replaced and supplemented with vehicle control, 50 ng/mL recombinant human IL-6 (BioLegend #570804), 50 ng/mL recombinant human IL-8 (BioLegend #574204), or both. Cells were incubated for 1 hour, then rinsed and collected. Cell pellets were lysed in RIPA buffer (150 mM NaCl, 1% TritonX-100, 0.5% sodium deoxycholate, 0.1% SDS, 50 mM Tris pH 8.0) supplemented with protease inhibitor (Roche #11873580001) and phosphatase inhibitor (Roche #04906845001). Protein was separated by SDS-PAGE and transferred to PVDF membrane using the TransBlot Turbo (BioRad). Membranes were blocked in LI-COR Odyssey buffer (#927-50000) for 1 hour at room temperature. Primary antibody incubation was performed overnight in blocking buffer at 4 °C. Membranes were washed 3 times for 10 minutes each in TBST (50 mM Tris pH 7.5, 150 mM NaCl, 0.1% Tween-20), then secondary antibodies were applied in blocking buffer for one hour at room temperature. Membranes were washed again 3 times for 10 minutes each

in TBST. Bands were visualized using the LI-COR Odyssey Imaging System. Full details of primary and secondary antibodies are given in **Supplementary Tables ST4** and **ST5**.

IncuCyte live cell proliferation assays

HGSC cells were seeded at 3,000 cells per well into 96-well plates in standard RPMI media with 10% FBS and 1% pen/strep. After settling overnight, cells were washed with PBS and media was changed to HSCDA or CMA conditioned media supplemented with 1% FBS. Cells were then imaged for up to 96 h using an IncuCyte S3 live imaging system at the University of Colorado Cancer Center Cell Technologies Shared Resource (RRID: RRID:SCR_021982). Cell confluence in each image was measured using IncuCyte software and then normalized to confluence at 0 h to generate a “fold-growth” metric. Data are reported as the average fold growth ± SEM of three wells for each treatment condition.

Generation of HSCDA Proficient and Deficient Mice

The University of Colorado Institutional Animal Care and Use Committee (IACUC) approved all mouse studies. Tumor burden analysis was performed in bone marrow transplanted (recipient) wild-type C57BL/6J mice (Jackson Labs, strain #000664; RRID:IMSR_JAX:000664). HSCDA Deficient mice were generated by transplanting recipient mice with bone marrow from transgenic donor mice in which an adipocyte specific adiponectin gene promoter (AdipoQ-Cre) controls the expression of an attenuated diphtheria toxin (DTA). HSCDA Proficient mice were transplanted with bone marrow from donor mice encoding AdipoQ-Cre but lacking DTA. Prior to transplant, 8- to 12-week-old female recipient mice were myeloablated by a split 12 Gy dose of X-ray irradiation (6 Gy doses split by 4 hours). Irradiated mice were rescued with retroorbital injection of 1×10^6 donor cells to reestablish the hematopoietic niche. Donor cells were obtained from fresh bone marrow of transgenic animals which can produce mature adipocytes (AdipoQ-Cre) or lack mature adipocytes (AdipoQ-Cre-DTA). Adipocyte-deficient donor mice were generated by crossing animals in which Cre recombinase expression is directed by the adiponectin promoter (Jackson Labs #010803, B6;FVB-Tg(AdipoQ-cre)1Evdr/J; RRID:IMSR_JAX:010803) with mice in which the DTA gene is placed downstream of a floxed stop codon in the ROSA26 locus (Jackson Labs #010527, B6;129-Gt(ROSA)26Sortm1(DTA)Mrc/J; RRID:IMSR_JAX:010527). Cre-mediated excision of the stop codon initiates DTA expression and cell death, which is restricted to mature

adipocytes by the adiponectin promoter. Adipocyte proficient donor mice are the result of the same cross, excluding the DTA gene. Recipient mice recover from bone marrow transplantation in approximately 6 weeks and are ready for exposure to tumor cell protocols.

ID8 Animal Study

Six weeks after bone marrow transplant, 5 million ID8 cells (*Tp53-/-*, *Brca2-/-*, GFP-luciferase+,[56, 57]) were implanted into HSCDA Proficient and Deficient mice by intraperitoneal injection. At 39-days post-ID8 cell injection, mice were euthanized, ascites fluid was collected, and necropsy was performed to assess tumor burden. All tumors were collected and weighed, including omentum tumors and disseminated tumor nodules within the mesentery and other peritoneal tissues.

SO Animal Study

Eight weeks after bone marrow transplant, 20,000 SO cells (*Tp53-/-*, *Brca1/2* wild-type, $Hras^{V12}$ and *Myc* transformed) were implanted into HSCDA Proficient and Deficient mice by intraperitoneal injection. At 20-days post-SO cell injection, mice were euthanized and necropsy was performed to assess tumor burden. All tumors were collected and weighed, including omentum tumors and disseminated tumor nodules within the mesentery and other peritoneal tissues.

Bulk RNA-Seq of ID8 Murine Omentum Tumors

Library preparation and sequencing were performed by the University of Colorado Cancer Center Genomics Shared Resource (RRID:SCR_021984). Reads were analyzed by the University of Colorado Cancer Center Bioinformatics Core Facility (RRID:SCR_021983). RNA-Seq data were processed using the nf-core RNAseq pipeline (version 3.12.0; [58]). Briefly, Illumina adapters were removed using Cutadapt (version 3.4; [47]) as part of the trimgalore (0.6.7) package [48]. Reads were aligned using STAR (version 2.7.9a; [49]) to the Ensembl mouse transcriptome (GRCm39 release 104) and quantified using Salmon (version 1.10.1; [50]). Raw data with counts by gene was generated using tximport [51] on salmon quantified data. Normalized data was generated to counts per million [52]. Differential expression was calculated using the limma R package [53] comparing

Deficient to the Proficient sample groups. Volcano plot was generated with GraphPad Prism (ver. 10.2.3). Raw and processed RNA-Seq data was deposited in the Gene Expression Omnibus (GSE268528).

Multiplex Immunohistochemistry (mIHC) and Image Analysis

Tissues were formalin fixed overnight at room temperature, embedded in paraffin blocks using a tissue processor, and sectioned at 4 micron onto charged glass slides. Slides were deparaffinized, heat treated in antigen retrieval buffer, blocked, and incubated with primary antibodies (Tables 1 and 2), followed by horseradish peroxidase (HRP)-conjugated secondary antibody polymer, and HRP-reactive OPAL fluorescent reagents. The slides were stripped between each consecutive staining cycle with heat treatment in antigen retrieval buffer. Whole slide scans were collected with PhenoImager HT v2.0.0 software using the 20x objective and a 0.5-micron resolution. Regions of interest (ROIs) were selected and rescanned using the 20x objective and the multispectral imaging cube. Spectral references and unstained control images were measured and inForm software v3.0 was used to create a multispectral library reference. The multispectral images (.im3 files) were spectrally unmixed and analyzed with tissue segmentation, cell segmentation, and phenotyping using inForm software v3.0 (Akoya Biosciences). Exported data were compiled and summarized using PhenoptrReports (Akoya Biosciences). Full antibody details are given in **Supplementary Table ST6**.

Brightfield IHC and Image Analysis

Tissues were formalin fixed overnight at room temperature, then paraffin embedded in blocks using a tissue processor and sectioned onto glass slides. All slides were de-identified and whole slide scans were collected on Akoya Biosciences Vectra 3 scanner using the 20x objective by the Human Immune Monitoring Shared Resource (RRID:SCR_021985). The slides were then analyzed on QuPath (v. 0.5.1 x64). ROIs were drawn to encompass the whole tissue and background correction was done for H-DAB. For each stain, 4 ROIs were drawn for training sets and excluded from analysis for which cell and positive cell detect parameters could be identified. Cell detections were based on hematoxylin signal, with exclusions for minimum cell area and the inclusion of a median filter radius. Cell positivity was determined on DAB pixel intensity, and the percentage of positive cells was reported as the ratio of cells above a set DAB optical density mean to the total number of cells in the tissue.

Data were exported and analyzed in GraphPad Prism 10 v. 10.3.1.The analyst was blinded to treatment group information until after the analysis was complete to avoid bias.

DECLARATIONS

Ethics approval and consent to participate: All mouse studies were approved by the University of Colorado Institutional Animal Care and Use Committee (IACUC; protocols 157 [generation of HSCDA Proficient and Deficient mice] and 569 [syngeneic models of ovarian cancer]). The samples utilized for primary preadipocyte culture were obtained under approval by the Colorado Multiple Institutional Review Board (COMIRB) with written informed consent from all participants. Samples were obtained from participants enrolled in NCT02654925, NCT04043520 and NCT03396978 and shared in a de-identified manner for use in this investigation.

Consent for publication: N/A

Availability of data and materials: Data generated and/or analyzed during this study are available from the corresponding author upon reasonable request. RNA-Seq or other large datasets are deposited as described in Materials and Methods and are publicly available.

Competing interests: The authors declare that they have no competing interests.

Funding: This work was primarily supported by the Department of Defense Ovarian Cancer Research Program (ZLW, OC210257; SO, HT94252410193) and the Colorado Clinical & Translational Sciences Institute (ZLW, CCTSI CO-Pilot CO-J-20-006), with additional support by the Rivkin Center for Ovarian Cancer Research (ZLW, Pilot Study Award) as well as Institutional Research Grant #22-154-59 from the American Cancer Society to the University of Colorado Cancer Center (ZLW). Further support was provided by the American Cancer Society (BGB, RSG-19-129-01-DDC), the NCI (BGB, R37CA261987; ZLW, R03CA249571), NIDDK (KMG, K01DK109053), NIA (KMG and DJK, U54 AG062319), VA (SO, I01BX006020), and the Boettcher Foundation. Use of the University of Colorado Bioinformatics and Biostatistics Shared Resource (BBSR), Human Immune Monitoring Shared Resource (HIMSR), and the Cell Technologies Shared Resource (CTSR) was supported by NCI grant P30CA046934 and by NIH/NCATS Colorado CTSA grant UL1TR002535. This work was supported by the Alpine HPC system, which is jointly funded by the University of Colorado Boulder, the University of

Colorado Anschutz, Colorado State University, and the National Science Foundation (award 2201538). Use of the MD Anderson RPPA Core was supported by NCI CA16672 and R50CA221675.

Author's contributions:

ERW (co-first author): performed experiments, analyzed data, prepared manuscript

CAB (co-first author): performed experiments, analyzed data, prepared manuscript

FT: performed experiments, revised manuscript

VM: performed experiments, analyzed data

JKM: performed experiments

TMS: performed experiments

MPB: analyzed data, revised manuscript

MSR: provided study materials

RV: provided study materials, aided in study design

BC: provided study materials, revised manuscript

KRJ: analyzed data

KMG: provided study materials, aided in study design, revised manuscript

DJK: provided study materials, aided in study design

SO: provided study materials

BGB: provided study materials, aided in study design, data analysis and interpretation, revised manuscript

ZLW: designed the study, performed experiments, analyzed and interpreted data, prepared manuscript

Acknowledgments: We acknowledge philanthropic contributions from the Kay L. Dunton Endowed Memorial Professorship in Ovarian Cancer Research, the McClintock-Addlesperger Family, Karen M. Jennison, Don and Arlene Mohler Johnson Family, Michael Intagliata, Duane and Denise Suess, Mary Normandin, and Donald Engelstad. The authors acknowledge the anonymous donors who provided biopsies for use in generating adipocyte cultures. The corresponding author (Zachary L Watson) wishes to dedicate this manuscript in memory of Maggie Watson (1981-2022) and Mira Watson (2016-2022).

FIGURES

Woodruff and Bailey et al. 2024 - Fig. 1

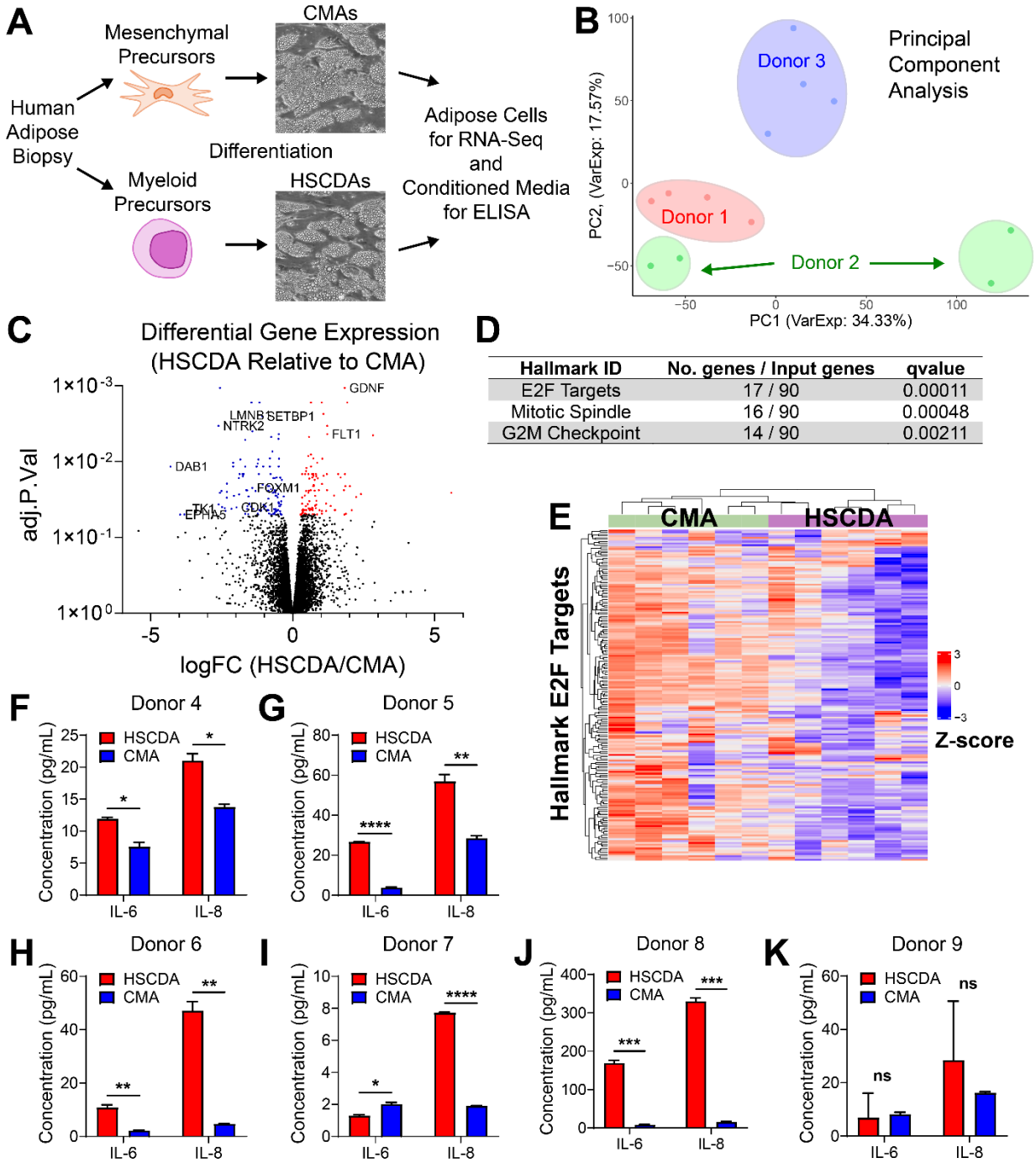

Hallmark ID	No. genes / Input genes	qvalue
E2F Targets	17 / 90	0.00011
Mitotic Spindle	16 / 90	0.00048
G2M Checkpoint	14 / 90	0.00211

Fig. 1. *In vitro* differentiated human primary HSCDAs exhibit unique transcription and cytokine secretion relative to CMAs. (A) Diagram of adipogenic differentiation of human primary precursor cells into HSCDAs and CMAs. Cell transcriptomes were analyzed by RNA-Seq. Conditioned media was analyzed by ELISA. **(B)** Principal component analysis (PCA) of adipocyte RNA-Seq. **(C)** Volcano plot of differential gene expression (DGE) comparing HSCDAs relative to CMAs. Specific gene names in E2F and other pathways are highlighted. **(D)** Significantly differentially regulated hallmark pathways. **(E)** Heatmap of Hallmark E2F Targets showing transcriptional downregulation of the pathway in HSCDAs relative to CMAs. **(F-K)** HSCDA or CMA conditioned media from six independent human donors was examined by ELISA for IL-6 and IL-8. Data are the average of two wells. Error bars = SD. T-test. * $p<0.05$, ** $p<0.01$, *** $p<0.001$, **** $p<0.0001$.

Woodruff and Bailey et al. 2024 - Fig. 2

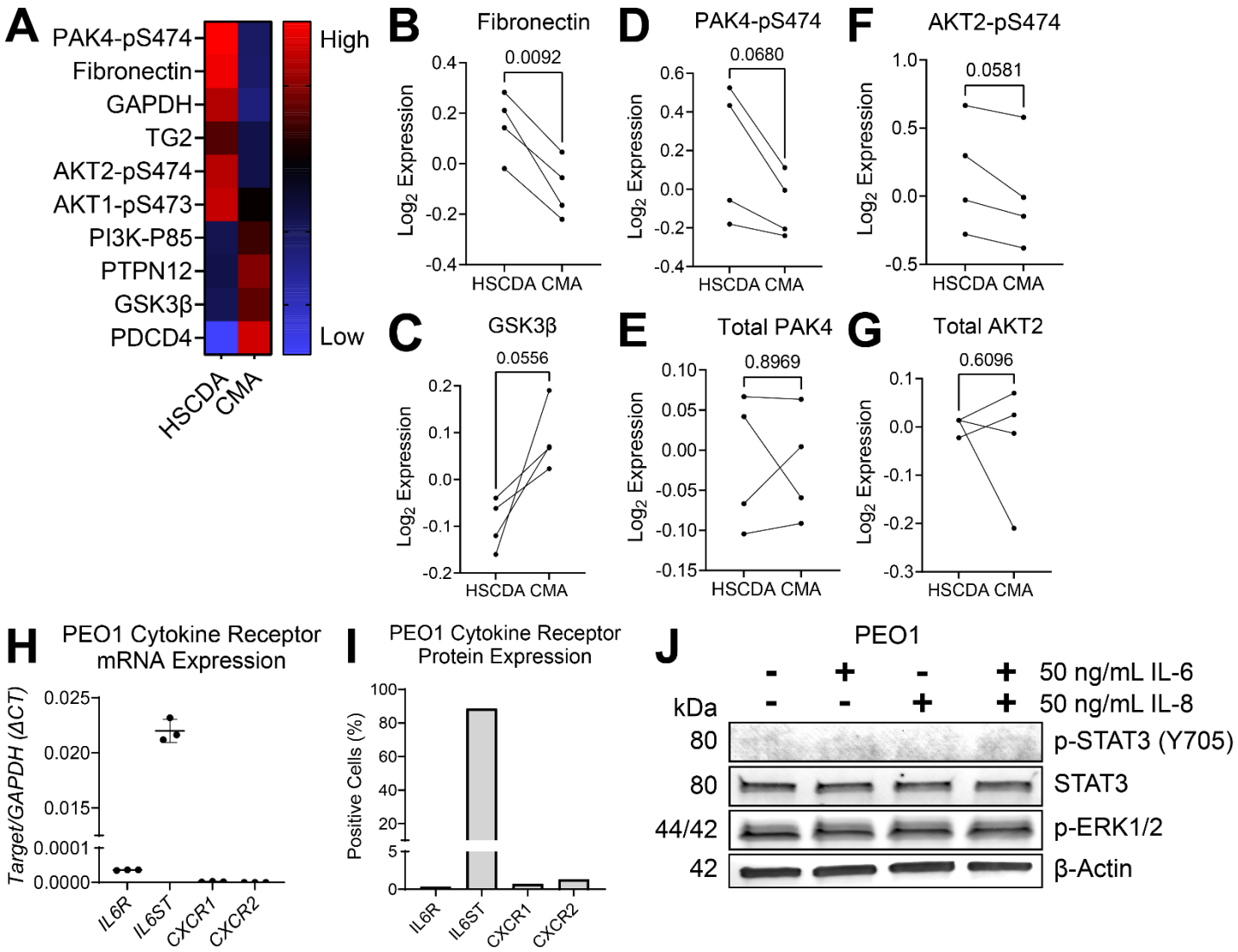

Fig. 2. PEO1 cells show differential protein expression and phosphorylation in HSCDA vs. CMA conditioned media. PEO1 cells were incubated in conditioned media from HSCDAs or CMAs for 24 hours. Protein expression and phosphorylation were examined by RPPA. **(A)** The heat map shows the average median centered Log_2 expression for PEO1 cells incubated in 4 independent media pairs (Donors 6 through 9). **(B-C)** Representative paired scatter plots showing consistent differential protein expression of fibronectin and GSK3β in PEO1 cells incubated in each media pair. **(D-G)** Paired scatter plots for phosphorylated and total forms of PAK4 and AKT2, showing differential regulation of serine phosphorylation, but not total protein. P-values by paired t-test. **(H)** RNA was isolated from PEO1 cells and RT-qPCR was performed for the indicated cytokine receptor transcripts. *GAPDH* was used for relative quantification. **(I)** Flow cytometry was performed on PEO1 cells to detect surface expression of the indicated cytokine receptor proteins. **(J)** PEO1 cells were grown with the indicated cytokine supplements for 1 hour. Immunoblots were performed for phosphorylated and total STAT3 (IL-6 signaling), phosphorylated ERK1/2 (IL-8 signaling), and β-actin loading control.

Woodruff and Bailey et al. 2024 - Fig. 3

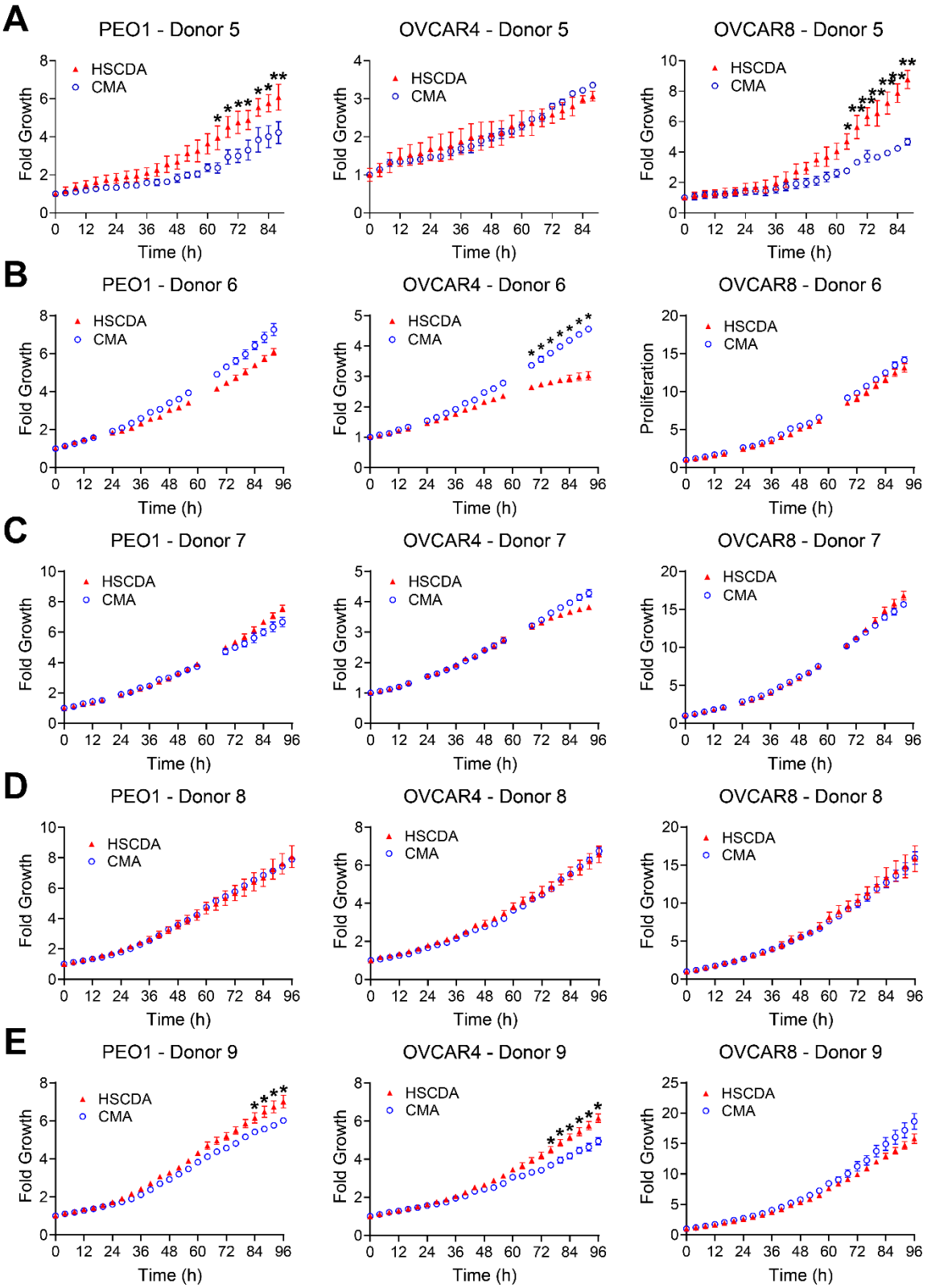

Fig. 3. HGSC cell proliferation in HSCDA vs CMA conditioned media. The listed HGSC cell lines were incubated in HSCDA or CMA conditioned media from five independent human donors **(A-E)**. Cell confluence was measured by IncuCyte live imaging and normalized to 0 hours to yield a "Fold Growth" metric. Each data point shows the mean ± SEM of 3 wells. * $p<0.05$, ** $p<0.01$.

Woodruff and Bailey et al. 2024 - Fig. 4

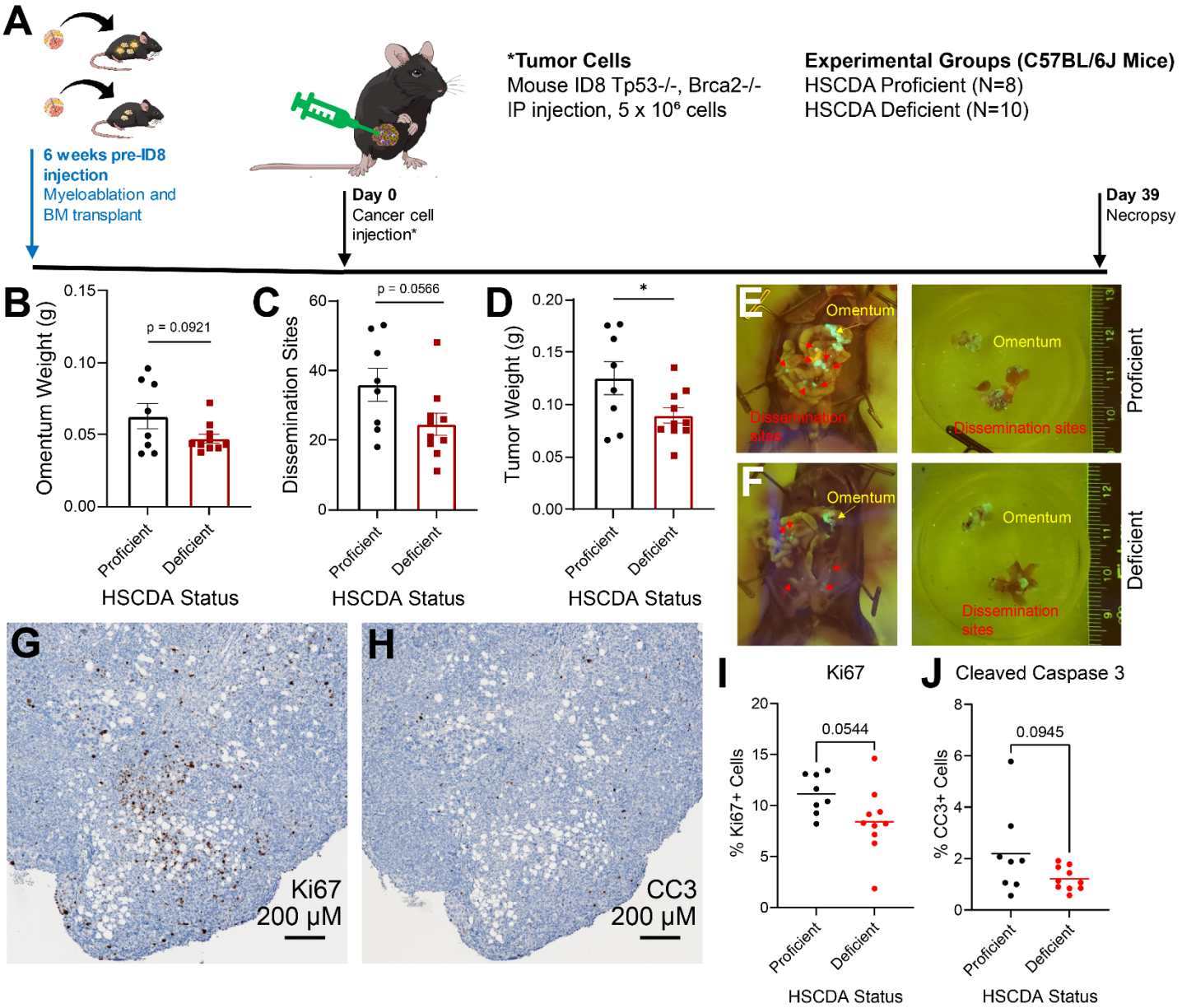

Fig. 4. Ablation of HSCDAs reduces tumor burden in the ID8 syngeneic mouse model of HGSC. (A) Experimental timeline, including bone marrow transplant and subsequent tumor study. **(B)** Weight of omental tumors. **(C)** Number of disseminated tumor nodules. **(D)** Weight of disseminated tumor nodules. For **(B-D)**, graphs show individual data points with mean ± SEM. p-values by unpaired T-test. * $p<0.05$. **(E-F)** Representative images of tumor burden in the peritoneal cavity of HSCDA Proficient and Deficient mice. **(G-H)** Representative images of ID8 omental tumor staining for Ki67 and cleaved caspase 3. **(I-J)** The percentage of Ki67-positive and cleaved caspase 3-positive tumor cells was determined using QuPath software. For **(I-J)**, graphs show individual data points with means (horizontal bar). p-values by unpaired T-test.

Woodruff and Bailey et al. 2024 - Fig. 5

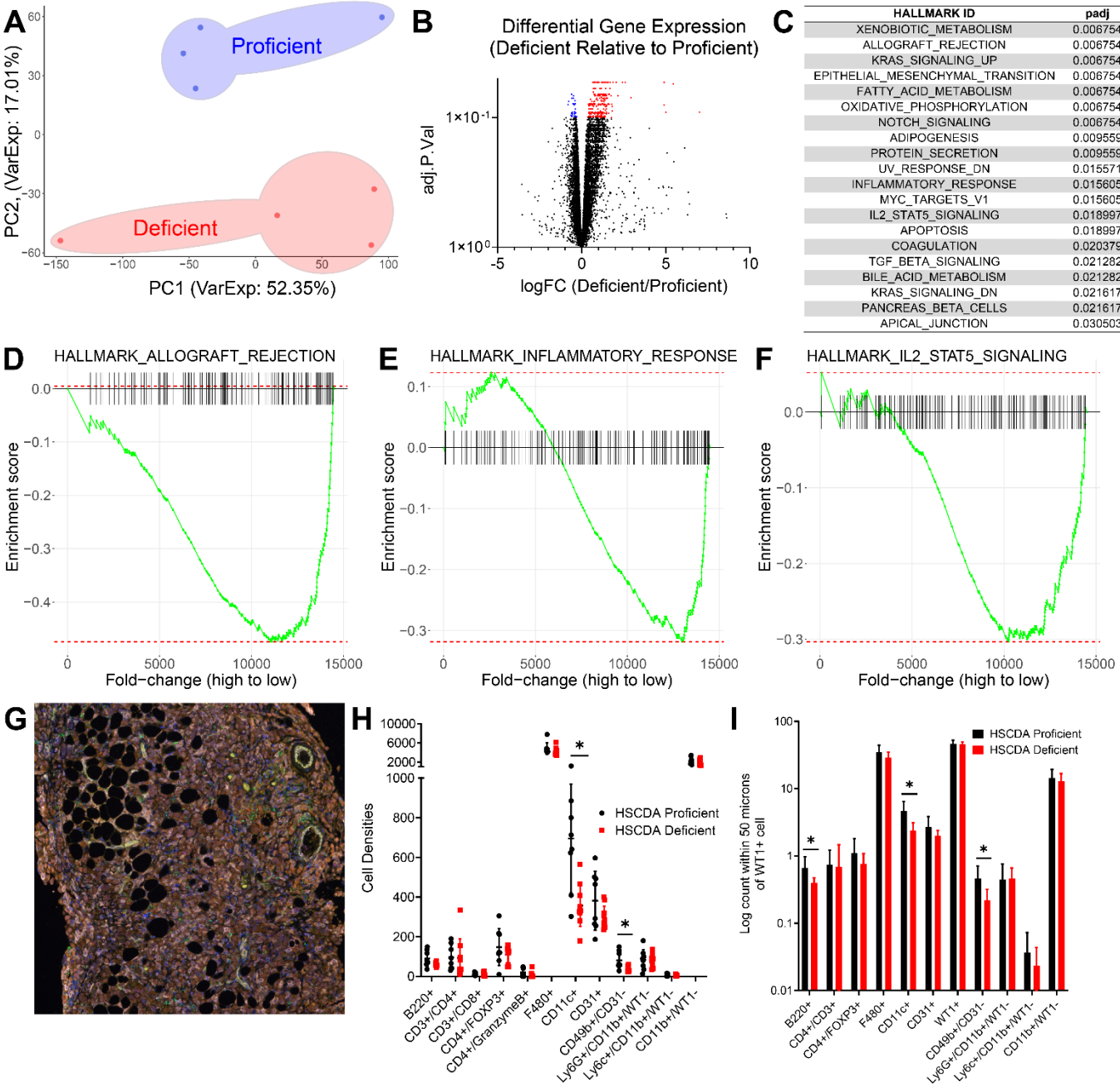

C

HALLMARK ID	padj	NES
XENOBIOTIC_METABOLISM	0.006754	-1.6101
ALLOGRAFT_REJECTION	0.006754	-2.1533
KRAS_SIGNALING_UP	0.006754	-1.60267
EPITHELIAL_MESENCHYMAL_TRANSITION	0.006754	-1.69105
FATTY_ACID_METABOLISM	0.006754	-1.59835
OXIDATIVE_PHOSPHORYLATION	0.006754	-1.97444
NOTCH_SIGNALING	0.006754	-1.98139
ADIPOGENESIS	0.009559	-1.50634
PROTEIN_SECRETION	0.009559	-1.61366
UV_RESPONSE_DN	0.015571	-1.54007
INFLAMMATORY_RESPONSE	0.015605	-1.45088
MYC_TARGETS_V1	0.015605	-1.38771
IL2_STAT5_SIGNALING	0.018997	-1.39293
APOPTOSIS	0.018997	-1.46009
COAGULATION	0.020379	-1.4758
TGF_BETA_SIGNALING	0.021282	-1.64548
BILE_ACID_METABOLISM	0.021282	-1.52442
KRAS_SIGNALING_DN	0.021617	1.524156
PANCREAS_BETA_CELLS	0.021617	-1.79148
APICAL_JUNCTION	0.030503	-1.33646

Fig. 5. Ablation of HSCDAs in mice alters ID8 omental tumor transcription and the tumor immune microenvironment. (A) Principal component analysis of ID8 omental tumor RNA-Seq from HSCDA Proficient (n=4) and Deficient (n=4) mice. **(B)** Volcano plot of overall RNA-Seq gene expression in HSCDA Deficient mice relative to Proficient mice (i.e., positive values indicate greater expression in Deficient mice). **(C)** Significantly differentially regulated hallmark pathways by GSEA. padj = p value adjusted for multiple comparisons. NES = Normalized Enrichment Score (adjusted for multiple comparisons). A positive NES indicates over-enrichment of pathway genes in HSCDA Deficient mice relative to Proficient mice, while a negative NES indicates under-enrichment in HSCDA Deficient mice relative to Proficient. **(D-F)** GSEA enrichment plots for Allograft Rejection, Inflammatory Response, and IL2-STAT5 Signaling. The U-shaped plots correspond to negative NES. **(G)** Sample image of multispectral IHC imaging of a mouse omental tumor. **(H)** Quantification of cell densities in omental tumors. **(I)** Quantification of the number of the indicated immune cells within 50 microns of a WT1+ tumor cell. Error bars = SD. T-test. * $p<0.05$.

TABLES

Table 1: Multiplex IHC Antibody Panel for Innate/Myeloid Mouse Immune Cells

Antibody	Marker Expression
CD11b	Myeloid cells
CD11c	Dendritic cells
Ly6c	Monocytic MDSCs
Ly6g	Granulocytic MDSCs
CD49b	NK and endothelial cells
CD31	Endothelial cells
F4/80	Macrophages
WT1	ID8 tumor cells
DAPI	Nuclei

Table 2: Multiplex IHC Antibody Panel for Adaptive/Lymphoid Mouse Immune Cells

Antibody	Marker Expression
CD3	T-cells
CD4	Helper T-cells
CD8	Cytotoxic T-cells
Granzyme B	Effector T-cells
FOXP3	Regulatory T-cells
B220	B-cells
WT1	ID8 tumor cells
DAPI	Nuclei

REFERENCES

1. Jayson, G.C., E.C. Kohn, H.C. Kitchener, and J.A. Ledermann, *Ovarian cancer.* Lancet, 2014. **384**(9951): p. 1376-88.
2. Gerber, S.A., V.Y. Rybalko, C.E. Bigelow, A.A. Lugade, T.H. Foster, J.G. Frelinger, and E.M. Lord, *Preferential attachment of peritoneal tumor metastases to omental immune aggregates and possible role of a unique vascular microenvironment in metastatic survival and growth.* Am J Pathol, 2006. **169**(5): p. 1739-52.
3. Swisher, E.M., R.L. Garcia, M.R. Kilgore, and B.M. Norquist, *Culprit or Bystander? The Role of the Fallopian Tube in "Ovarian" High-Grade Serous Carcinoma.* Cancer Discov, 2016. **6**(12): p. 1309-1311.
4. Dai, L., K. Song, and W. Di, *Adipocytes: active facilitators in epithelial ovarian cancer progression?* J Ovarian Res, 2020. **13**(1): p. 115.
5. Motohara, T., K. Masuda, M. Morotti, Y. Zheng, S. El-Sahhar, K.Y. Chong, N. Wietek, A. Alsaadi, E.M. Carrami, Z. Hu, M. Artibani, L.S. Gonzalez, H. Katabuchi, H. Saya, and A.A. Ahmed, *An evolving story of the metastatic voyage of ovarian cancer cells: cellular and molecular orchestration of the adipose-rich metastatic microenvironment.* Oncogene, 2019. **38**(16): p. 2885-2898.
6. Meza-Perez, S. and T.D. Randall, *Immunological Functions of the Omentum.* Trends Immunol, 2017. **38**(7): p. 526-536.
7. Cleypool, C.G.J., B. Schurink, D.E.M. van der Horst, and R. Bleys, *Sympathetic nerve tissue in milky spots of the human greater omentum.* J Anat, 2020. **236**(1): p. 156-164.
8. Ladanyi, A., A. Mukherjee, H.A. Kenny, A. Johnson, A.K. Mitra, S. Sundaresan, K.M. Nieman, G. Pascual, S.A. Benitah, A. Montag, S.D. Yamada, N.A. Abumrad, and E. Lengyel, *Adipocyte-induced CD36 expression drives ovarian cancer progression and metastasis.* Oncogene, 2018. **37**(17): p. 2285-2301.
9. Nieman, K.M., H.A. Kenny, C.V. Penicka, A. Ladanyi, R. Buell-Gutbrod, M.R. Zillhardt, I.L. Romero, M.S. Carey, G.B. Mills, G.S. Hotamisligil, S.D. Yamada, M.E. Peter, K. Gwin, and E. Lengyel, *Adipocytes promote ovarian cancer metastasis and provide energy for rapid tumor growth.* Nat Med, 2011. **17**(11): p. 1498-503.
10. Nieman, K.M., I.L. Romero, B. Van Houten, and E. Lengyel, *Adipose tissue and adipocytes support tumorigenesis and metastasis.* Biochim Biophys Acta, 2013. **1831**(10): p. 1533-41.
11. Mikula-Pietrasik, J., P. Uruski, P. Sosinska, K. Maksin, H. Piotrowska-Kempisty, M. Kucinska, M. Murias, S. Szubert, A. Wozniak, D. Szpurek, S. Sajdak, K. Piwocka, A. Tykarski, and K. Ksiazek, *Senescent peritoneal mesothelium creates a niche for ovarian cancer metastases.* Cell Death Dis, 2016. **7**(12): p. e2565.
12. Crossno, J.T., Jr., S.M. Majka, T. Grazia, R.G. Gill, and D.J. Klemm, *Rosiglitazone promotes development of a novel adipocyte population from bone marrow-derived circulating progenitor cells.* J Clin Invest, 2006. **116**(12): p. 3220-8.
13. Gavin, K.M., T.M. Sullivan, J.K. Maltzahn, M.R. Jackman, A.E. Libby, P.S. MacLean, W.M. Kohrt, S.M. Majka, and D.J. Klemm, *Hematopoietic Stem Cell-Derived Adipocytes Modulate Adipose Tissue Cellularity, Leptin Production and Insulin Responsiveness in Female Mice.* Front Endocrinol (Lausanne), 2022. **13**: p. 844877.
14. Ryden, M., M. Uzunel, J.L. Hard, E. Borgstrom, J.E. Mold, E. Arner, N. Mejhert, D.P. Andersson, Y. Widlund, M. Hassan, C.V. Jones, K.L. Spalding, B.M. Svahn, A. Ahmadian, J. Frisen, S. Bernard, J. Mattsson, and P. Arner, *Transplanted Bone Marrow-Derived Cells Contribute to Human Adipogenesis.* Cell Metab, 2015. **22**(3): p. 408-17.
15. Gavin, K.M., J.A. Gutman, W.M. Kohrt, Q. Wei, K.L. Shea, H.L. Miller, T.M. Sullivan, P.F. Erickson, K.M. Helm, A.S. Acosta, C.R. Childs, E. Musselwhite, M. Varella-Garcia, K. Kelly, S.M. Majka, and D.J. Klemm, *De novo generation of adipocytes from circulating progenitor cells in mouse and human adipose tissue.* Faseb j, 2016. **30**(3): p. 1096-108.
16. Gavin, K.M., S.M. Majka, W.M. Kohrt, H.L. Miller, T.M. Sullivan, and D.J. Klemm, *Hematopoietic-to-mesenchymal transition of adipose tissue macrophages is regulated by integrin beta1 and fabricated fibrin matrices.* Adipocyte, 2017. **6**(3): p. 234-249.
17. Gavin, K.M., T.M. Sullivan, W.M. Kohrt, S.M. Majka, and D.J. Klemm, *Ovarian Hormones Regulate the Production of Adipocytes From Bone Marrow-Derived Cells.* Front Endocrinol (Lausanne), 2018. **9**: p. 276.

18. Gavin, K.M., B. Conrad, T. Sullivan, R. Vianzon, A.S. Acosta, W.M. Kohrt, and D.J. Klemm, *Adipogenic differentiation of hematopoietic lineage cells isolated from adipose tissue of humans.* bioRxiv, 2024: p. 2024.06.22.600230.
19. Majka, S.M., K.E. Fox, J.C. Psilas, K.M. Helm, C.R. Childs, A.S. Acosta, R.C. Janssen, J.E. Friedman, B.T. Woessner, T.R. Shade, M. Varella-Garcia, and D.J. Klemm, *De novo generation of white adipocytes from the myeloid lineage via mesenchymal intermediates is age, adipose depot, and gender specific.* Proc Natl Acad Sci U S A, 2010. **107**(33): p. 14781-6.
20. Guo, Q.Y., J.N. Song, Y.M. Chen, H.N. Yuan, W.S. Xue, Y. Sun, X.L. Niu, Y. Wang, and X. Chen, *IL-6 regulates epithelial ovarian cancer EMT, invasion, and metastasis by modulating Let-7c and miR-200c through the STAT3/HIF-1α pathway.* Med Oncol, 2024. **41**(6): p. 155.
21. Lee, J., Y. Han, S. Kim, H. Jo, W. Wang, U. Cho, S.I. Kim, B. Kim, and Y.S. Song, *Mitochondrial fission enhances IL-6-induced metastatic potential in ovarian cancer via ERK1/2 activation.* Cancer Sci, 2024. **115**(5): p. 1536-1550.
22. Nguyen, L.L., Z.L. Watson, R. Ortega, E.R. Woodruff, K.R. Jordan, R. Iwanaga, T.M. Yamamoto, C.A. Bailey, F. To, A.D. Jeong, S.R. Guntupalli, K. Behbakht, V. Gibaja, N. Arnoult, A. Cocozaki, E.B. Chuong, and B.G. Bitler, *Combining EHMT and PARP Inhibition: A Strategy to Diminish Therapy-Resistant Ovarian Cancer Tumor Growth while Stimulating Immune Activation.* Mol Cancer Ther, 2024.
23. Noone AM, H.N., Krapcho M, Miller D, Brest A, Yu M, Ruhl J, Tatalovich Z, Mariotto A, Lewis DR, Chen HS, Feuer EJ, Cronin KA, *SEER Cancer Statistics Review, 1975-2015*. 2018, National Cancer Institute, Bethesda, MD.
24. Harper, E.I., E.F. Sheedy, and M.S. Stack, *With Great Age Comes Great Metastatic Ability: Ovarian Cancer and the Appeal of the Aging Peritoneal Microenvironment.* Cancers (Basel), 2018. **10**(7).
25. Shao, M., L. Cao, C. Shen, M. Satpathy, B. Chelladurai, R.M. Bigsby, H. Nakshatri, and D. Matei, *Epithelial-to-mesenchymal transition and ovarian tumor progression induced by tissue transglutaminase.* Cancer Res, 2009. **69**(24): p. 9192-201.
26. Cao, L., M. Shao, J. Schilder, T. Guise, K.S. Mohammad, and D. Matei, *Tissue transglutaminase links TGF-β, epithelial to mesenchymal transition and a stem cell phenotype in ovarian cancer.* Oncogene, 2012. **31**(20): p. 2521-34.
27. Lin, T.C., C.H. Yang, L.H. Cheng, W.T. Chang, Y.R. Lin, and H.C. Cheng, *Fibronectin in Cancer: Friend or Foe.* Cells, 2019. **9**(1).
28. Abo, A., J. Qu, M.S. Cammarano, C. Dan, A. Fritsch, V. Baud, B. Belisle, and A. Minden, *PAK4, a novel effector for Cdc42Hs, is implicated in the reorganization of the actin cytoskeleton and in the formation of filopodia.* Embo j, 1998. **17**(22): p. 6527-40.
29. Chetty, A.K., B.H. Ha, and T.J. Boggon, *Rho family GTPase signaling through type II p21-activated kinases.* Cell Mol Life Sci, 2022. **79**(12): p. 598.
30. Li, Y., Y. Shao, Y. Tong, T. Shen, J. Zhang, Y. Li, H. Gu, and F. Li, *Nucleo-cytoplasmic shuttling of PAK4 modulates β-catenin intracellular translocation and signaling.* Biochim Biophys Acta, 2012. **1823**(2): p. 465-75.
31. Villa-Moruzzi, E., *Tyrosine phosphatases in the HER2-directed motility of ovarian cancer cells: Involvement of PTPN12, ERK5 and FAK.* Anal Cell Pathol (Amst), 2011. **34**(3): p. 101-12.
32. Villa-Moruzzi, E., *PTPN12 controls PTEN and the AKT signalling to FAK and HER2 in migrating ovarian cancer cells.* Mol Cell Biochem, 2013. **375**(1-2): p. 151-7.
33. Gao, F., X. Wang, F. Zhu, Q. Wang, X. Zhang, C. Guo, C. Zhou, C. Ma, W. Sun, Y. Zhang, Y.H. Chen, and L. Zhang, *PDCD4 gene silencing in gliomas is associated with 5'CpG island methylation and unfavourable prognosis.* J Cell Mol Med, 2009. **13**(10): p. 4257-67.
34. Long, J., Y. Yin, H. Guo, S. Li, Y. Sun, C. Zeng, and W. Zhu, *The mechanisms and clinical significance of PDCD4 in colorectal cancer.* Gene, 2019. **680**: p. 59-64.
35. Cardenas, C., M.K. Montagna, M. Pitruzzello, E. Lima, G. Mor, and A.B. Alvero, *Adipocyte microenvironment promotes Bclxl expression and confers chemoresistance in ovarian cancer cells.* Apoptosis, 2017. **22**(4): p. 558-569.
36. Qu, Q., L. Liu, Y. Cui, Y. Chen, Y. Wang, and Y. Wang, *Exosomes from Human Omental Adipose-Derived Mesenchymal Stem Cells Secreted into Ascites Promote Peritoneal Metastasis of Epithelial Ovarian Cancer.* Cells, 2022. **11**(21).
37. Ferrante, S.C., E.P. Nadler, D.K. Pillai, M.J. Hubal, Z. Wang, J.M. Wang, H. Gordish-Dressman, E. Koeck, S. Sevilla, A.A. Wiles, and R.J. Freishtat, *Adipocyte-derived exosomal miRNAs: a novel mechanism for obesity-related disease.* Pediatr Res, 2015. **77**(3): p. 447-54.

38. Thomou, T., M.A. Mori, J.M. Dreyfuss, M. Konishi, M. Sakaguchi, C. Wolfrum, T.N. Rao, J.N. Winnay, R. Garcia-Martin, S.K. Grinspoon, P. Gorden, and C.R. Kahn, *Adipose-derived circulating miRNAs regulate gene expression in other tissues.* Nature, 2017. **542**(7642): p. 450-455.
39. Cheng, Y. and W. Liu, *MicroRNA-503 serves an oncogenic role in retinoblastoma progression by directly targeting PTPN12.* Exp Ther Med, 2019. **18**(3): p. 2285-2292.
40. Li, L., X. Zhang, Z. Yi, X. Liang, W. Yin, and S. Li, *MiR-503 promotes the migration and invasion of colorectal cancer cells by regulating PDCD4.* J buon, 2018. **23**(3): p. 579-586.
41. Montfort, A., O. Pearce, E. Maniati, B.G. Vincent, L. Bixby, S. Böhm, T. Dowe, E.H. Wilkes, P. Chakravarty, R. Thompson, J. Topping, P.R. Cutillas, M. Lockley, J.S. Serody, M. Capasso, and F.R. Balkwill, *A Strong B-cell Response Is Part of the Immune Landscape in Human High-Grade Serous Ovarian Metastases.* Clin Cancer Res, 2017. **23**(1): p. 250-262.
42. Bassani, B., D. Baci, M. Gallazzi, A. Poggi, A. Bruno, and L. Mortara, *Natural Killer Cells as Key Players of Tumor Progression and Angiogenesis: Old and Novel Tools to Divert Their Pro-Tumor Activities into Potent Anti-Tumor Effects.* Cancers (Basel), 2019. **11**(4).
43. Dean, I., C.Y.C. Lee, Z.K. Tuong, Z. Li, C.A. Tibbitt, C. Willis, F. Gaspal, B.C. Kennedy, V. Matei-Rascu, R. Fiancette, C. Nordenvall, U. Lindforss, S.M. Baker, C. Stockmann, V. Sexl, S.A. Hammond, S.J. Dovedi, J. Mjösberg, M.R. Hepworth, G. Carlesso, M.R. Clatworthy, and D.R. Withers, *Rapid functional impairment of natural killer cells following tumor entry limits anti-tumor immunity.* Nat Commun, 2024. **15**(1): p. 683.
44. Rosser, E.C. and C. Mauri, *Regulatory B cells: origin, phenotype, and function.* Immunity, 2015. **42**(4): p. 607-12.
45. Zhang, E., C. Ding, S. Li, X. Zhou, B. Aikemu, X. Fan, J. Sun, M. Zheng, and X. Yang, *Roles and mechanisms of tumour-infiltrating B cells in human cancer: a new force in immunotherapy.* Biomark Res, 2023. **11**(1): p. 28.
46. Ewels, P.A., A. Peltzer, S. Fillinger, H. Patel, J. Alneberg, A. Wilm, M.U. Garcia, P. Di Tommaso, and S. Nahnsen, *The nf-core framework for community-curated bioinformatics pipelines.* Nat Biotechnol, 2020. **38**(3): p. 276-278.
47. Kechin, A., U. Boyarskikh, A. Kel, and M. Filipenko, *cutPrimers: A New Tool for Accurate Cutting of Primers from Reads of Targeted Next Generation Sequencing.* J Comput Biol, 2017. **24**(11): p. 1138-1143.
48. sclamons, F.K.F.J.P.E.E.A.M.W.B.S.-B.G.H., *FelixKrueger/TrimGalore: v0.6.10 - add default decompression path.* 2023.
49. Dobin, A., C.A. Davis, F. Schlesinger, J. Drenkow, C. Zaleski, S. Jha, P. Batut, M. Chaisson, and T.R. Gingeras, *STAR: ultrafast universal RNA-seq aligner.* Bioinformatics, 2013. **29**(1): p. 15-21.
50. Patro, R., G. Duggal, M.I. Love, R.A. Irizarry, and C. Kingsford, *Salmon provides fast and bias-aware quantification of transcript expression.* Nat Methods, 2017. **14**(4): p. 417-419.
51. Soneson, C., M.I. Love, and M.D. Robinson, *Differential analyses for RNA-seq: transcript-level estimates improve gene-level inferences.* F1000Res, 2015. **4**: p. 1521.
52. Robinson, M.D., D.J. McCarthy, and G.K. Smyth, *edgeR: a Bioconductor package for differential expression analysis of digital gene expression data.* Bioinformatics, 2010. **26**(1): p. 139-40.
53. Ritchie, M.E., B. Phipson, D. Wu, Y. Hu, C.W. Law, W. Shi, and G.K. Smyth, *limma powers differential expression analyses for RNA-sequencing and microarray studies.* Nucleic Acids Res, 2015. **43**(7): p. e47.
54. Korotkevich, G., V. Sukhov, N. Budin, B. Shpak, M.N. Artyomov, and A. Sergushichev, *Fast gene set enrichment analysis.* bioRxiv, 2021: p. 060012.
55. Liberzon, A., A. Subramanian, R. Pinchback, H. Thorvaldsdóttir, P. Tamayo, and J.P. Mesirov, *Molecular signatures database (MSigDB) 3.0.* Bioinformatics, 2011. **27**(12): p. 1739-40.
56. Walton, J., J. Blagih, D. Ennis, E. Leung, S. Dowson, M. Farquharson, L.A. Tookman, C. Orange, D. Athineos, S. Mason, D. Stevenson, K. Blyth, D. Strathdee, F.R. Balkwill, K. Vousden, M. Lockley, and I.A. McNeish, *CRISPR/Cas9-Mediated Trp53 and Brca2 Knockout to Generate Improved Murine Models of Ovarian High-Grade Serous Carcinoma.* Cancer Res, 2016. **76**(20): p. 6118-6129.
57. Nguyen, L.L., Z.L. Watson, R. Ortega, E.R. Woodruff, K.R. Jordan, R. Iwanaga, T.M. Yamamoto, C.A. Bailey, F. To, S. Lin, F.R. Villagomez, A.D. Jeong, S.R. Guntupalli, K. Behbakht, V. Gibaja, N. Arnoult, E.B. Chuong, and B.G. Bitler, *EHMT1/2 inhibition promotes regression of therapy-resistant ovarian cancer tumors in a CD8 T cell-dependent manner.* Mol Cancer Res, 2024.
58. *nf-core/rnaseq: nf-core/rnaseq v3.14.0 - Hassium Honey Badger.* 2024.